

Stability of branched tubular membrane structures

Maike Jung,^{1,*} Gerhard Jung,² and Friederike Schmid^{1,†}

¹*Institut für Physik, Johannes Gutenberg-Universität Mainz, Staudingerweg 9, 55128 Mainz, Germany*

²*Laboratoire Charles Coulomb (L2C), Université de Montpellier, CNRS, 34095 Montpellier, France*

We study the energetics and stability of branched tubular membrane structures by computer simulations of a triangulated network model. We find that triple (Y-)junctions can be created and stabilized by applying mechanical forces, if the angle between branches is 120° . The same holds for tetrahedral junctions with tetraeder angles. If the wrong angles are enforced, the branches coalesce to a linear structure, a pure tube. After releasing the mechanical force, Y-branched structures remain metastable if one constrains the enclosed volume and the average curvature (the area difference) to a fixed value; tetrahedral junctions however split up into two Y-junctions. Somewhat counterintuitively, the energy cost of adding a Y-branch is negative in structures with fixed surface area and tube diameter, even if one accounts for the positive contribution of the additional branch end. For fixed average curvature, however, adding a branch also enforces a thinning of tubes, therefore the overall curvature energy cost is positive. Possible implications for the stability of branched networks structures in cells are discussed.

Tubular membrane network structures are abundant in biological cells, for example in the Golgi complex [1, 2] and the endoplasmic reticulum [3, 4]. Such tubular networks are highly dynamic structures [5], in which new tubes are constantly created and existing tubes are merged or dissolved. Potential physiological roles of the three-dimensional tubular network spanning the endoplasmic reticulum include membrane trafficking, lipid metabolism and autophagy, i.e. the cleaning mechanism of the cell [4]. The function of the tubular network in the Golgi apparatus appears to be the interconnection of different building blocks, which can also induce structural rearrangements during cell differentiation [6]. Membrane nanotubes have also been found to generally enhance intercellular transport [7]. Understanding the formation and stability of tubular networks is thus a critical problem in the fields of biology, biophysics and soft matter.

The formation of tubular structures and membrane networks can be induced by various different mechanisms, which can be classified into different categories [8]. The most obvious way of creating tubular structures is by a force acting on a localized point on the membrane surface. This force can be induced by growing filaments (filament bundles) which are attached to the membrane [9, 10] or by a concerted action of molecular motors [11–16]. Other mechanisms for tube formation include scaffolding, in which proteins are polymerizing on the surface of the membrane, effectively forcing the membrane to adopt the shape of the proteins [17, 18], and the adsorption or inclusion of curvature-inducing proteins, which have been widely observed in nature [19, 20] and can induce either positive or negative curvature [21, 22]. For example, reticulon has been found to induce the tubular network structure in the endoplasmic reticulum [23–25].

From a theoretical point of view, membrane shapes have been studied intensely for many decades [26–28],

often using elastic continuum models based on the Canham-Helfrich theory [29–31]. Already for structures with simple sphere topology, the shape diagrams were found to be surprisingly complex, with first and second order transitions between prolate, oblate, pear and stomatocyte shapes [26, 32–34]. The process of mechanically pulling tubes from vesicles has been investigated in detail by experiment, theory and simulation [35–42] and found to be accompanied by a free energy barrier [39], suggesting that it might be possible to create metastable tubular structures using mechanical forces (e.g., molecular motors). Indeed, Bahrami et al [43] have recently demonstrated by computer simulations that linear tubular structures can be metastable even in the absence of forces and curvature-inducing proteins, as long as the enclosed volume is kept fixed. This is due to the existence of a free energy barrier between the linear tube shape and the true minimum-energy shapes, which are oblate and prolate structures for thick tubes and stomatocytes in the case of thin tubes.

While the (meta)stability of linear tubular structures has been analyzed in some detail, a network has a second fundamental building block, i.e. the junctions where several tubes merge. Detailed theoretical analyses of such branched structures, comparable to the ones for cylindrical tubes, however, are still missing. In the present Letter, we aim to fill this gap. We will first consider force-stabilized branched structures and examine their stability. Then we will establish conditions under which force-free branched structures can be metastable.

Model and method. Our starting point is the simplest continuum description of two-dimensional fluid membranes on large scales, the so-called Helfrich Hamiltonian [29–31].

$$H_{cv} = \frac{\kappa}{2} \int dA K^2 + \bar{\kappa} \int dA K_G. \quad (1)$$

Here κ , $\bar{\kappa}$ are curvature moduli (for lipid membranes, κ is typically of order $20k_B T$ [44]), K is the total curvature, and K_G the Gaussian curvature. We consider closed

* maike.lauf@web.de

† friederike.schmid@uni-mainz.de

structures with fixed sphere topology, hence the last term is a constant according to the Gauss-Bonnet theorem [45] and can be omitted. We note that we have not included a spontaneous curvature term in Eq. (1). Instead, we will discuss the effect of imposing an integrated average curvature $\int dA K$ in the spirit of the area difference elasticity (ADE) model [46–49]. The physical origin of this global curvature could be asymmetric numbers of lipid in the inner and outer membrane leaflet (“area difference”) [31, 46–52].

The theory is solved numerically using a dynamically-triangulated surface model [43, 53–64]. Specifically, we use the version of Noguchi and Gompper [65] which is described in detail in Ref. [66]. The surface is described by a network of N vertices that are connected by bonds in a triangular network structure ($N_\Delta = 2(N - 2)$ triangles), and the simulation is a combination of Brownian dynamics (node motion) and Monte Carlo moves (bond flips). We fix the area ($A = A_0$) and in some simulations also the enclosed volume V and the dimensionless average curvature (the area difference) [43, 46–49] $\Delta a = \frac{1}{4\sqrt{\pi A_0}} \int dA K$ by introducing harmonic constraint potentials with spring constants k_A, k_V , and $k_{\Delta a}$. Details of the implementation can be found in Supplementary Information (SI).

In the following, results are given in units of l_b (typical bond length), $\epsilon = \frac{\kappa}{20}$ (energy unit) and $\tau = l_b \sqrt{m\epsilon^{-1}}$ (time unit), where m is the mass of the vertices. Unless stated otherwise, the remaining parameters are $k_B T = 1\epsilon$, $N = 2562$, $A_0 = 0.41 l_b^2 \cdot N_\Delta$, $k_A = 2\epsilon/l_b^2$, $k_V = k_{\Delta a} = 0$, and the simulation time step is $\Delta t = 10^{-4}\tau$. Constraints on V and/or Δa are imposed by setting $k_V = 1\epsilon/l_b^3$ and/or $k_{\Delta a} = 1\epsilon$. The enclosed volume will be characterized by the dimensionless quantity $\nu = 6\sqrt{\pi/A^3}V$. The reference values of ν and Δa for perfect spheres are thus $\nu = \Delta a = 1$.

Force-stabilized linear and branched tubular structures. To create tubular structures, forces with amplitude F_{ext} are applied to a set of n vertices such that the total force is zero ($n = 2, 3, 4$). For $n = 2$, linear tubes are obtained. For $n = 3$, a branched structure with a Y-junction can be stabilized, provided the forces lie in one plane and have an angle of 120° to each other (see Fig. 1a), otherwise one creates linear structures as well. Using $n = 4$, one can create mechanically forced tetrahedral junctions; all other four-fold junctions are unstable and separate into Y-junctions (see SI, Fig. 1 and movies `4fold.mp4`, `4fold_twisted.mp4`, `tetrahedral.mp4`).

Y-junctions with fixed angle 120° are characteristic of the so-called Fermat point, the state that minimizes the total tube length of a network if the tube ends are kept at fixed positions. In experimental studies, artificial surfactant and liposome networks with fixed tube ends were found to always evolve towards the Fermat-point [67–69]. Our simulations show that these 120° Y-junctions remain the only stable triple junctions even in situations where the tube ends are mobile. Fig. 1b) shows the effect of slightly perturbing the angle of one applied force from

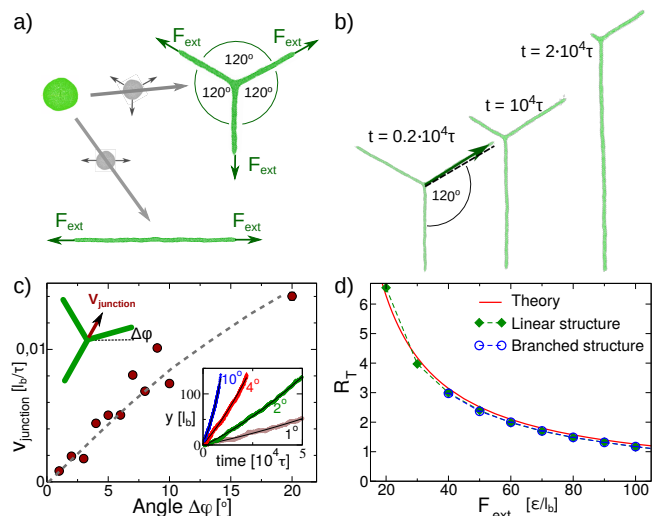


FIG. 1. Force-stabilized tubular structures. (a) Illustration of creation process. The starting point is a force-free spherical vesicle. To create linear structures, two opposing forces are applied at opposing vertices while keeping the area A fixed (no other constraints). Y-branched structures are obtained by applying three co-planar forces with angles 120° to each other. (b) Evolution of a Y-branched structure with time t at $F_{\text{ext}} = 90\epsilon/l_b$ if the direction of one applied force deviates from the symmetric direction by $\Delta\varphi = 4^\circ$ [70]. (c) Initial velocity of the junction as a function of $\Delta\varphi$ at $F_{\text{ext}} = 90\epsilon/l_b$. Dashed line is a guide for the eye. Inset shows the displacement y of the junction from its initial position versus time for different $\Delta\varphi$ as indicated, along with a quadratic fit to $y = y_0 + v_{\text{junction}}t + bt^2$ (black lines). (d) Tube radius versus applied force F_{ext} for linear (green diamond) and branched structures (blue circles), compared with theory (red line).

120° , starting from the configuration 1a): The junction starts moving in the direction of the smallest angle until it disappears, with a velocity that is roughly proportional to the distortion $\Delta\varphi$ (Fig. 1c).

For stable branched structures, the presence of the junction has little effect on the structure of the connected tubes. The tube radius R_T as a function of the applied force F_{ext} is the same for linear and branched structures and consistent with the theoretical estimate [11, 35] $R_T = 2\pi\kappa/F_{\text{ext}}$. (Fig. 1d).

Next we analyze the curvature energy (1) of the different structures. Fig. 2a) shows the results at temperature $k_B T = 1$ and after annealing to $k_B T = 10^{-6}\epsilon \approx 0$ for linear and branched structures. The energies at $k_B T = 1\epsilon$ and $k_B T \approx 0$ differ by roughly $N/2$, indicating that this energy difference can be attributed to thermal out-of-plane fluctuations of vertices. Interestingly, the elastic energy of branched structures is found to be *lower* than that of linear structures (Fig. 2a, lower panel).

To analyze this in more detail, we calculate separately the excess elastic energy of caps (tube ends) and junctions relative to a reference cylindrical tube section with the same radius and the same area (see Fig. 2c): We

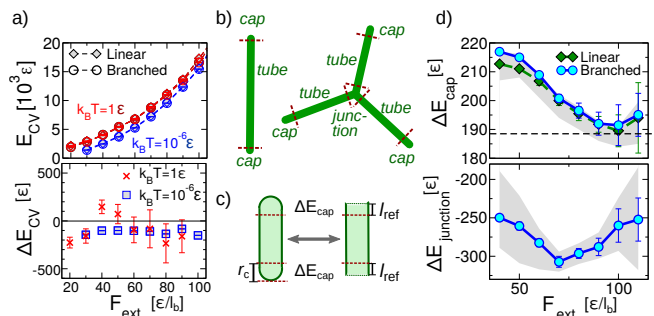


FIG. 2. Curvature energies of force-stabilized tubular structures. (a) Top: Elastic energy for linear (diamonds) and branched (circles) structures as a function of applied force F_{ext} at $k_B T = 1\epsilon$ (red) and $k_B T = 10^{-6}\epsilon$ (blue). Bottom: Difference between the curvature energy of branched and linear structures $k_B T = 1\epsilon$ (red crosses) and $k_B T = 10^{-6}\epsilon$ (blue squares). (b) Cartoon showing dissection of structures into tubes, caps and junctions (see text). (c) Cartoon illustrating the definition of excess energies: The energy of a tubular structure is compared to that of a reference tubular section with the same area. (d) Excess curvature energy of caps (top) and junctions (bottom) for linear (green diamonds) and branched (blue circles) structures, obtained at $k_B T = 10^{-6}\epsilon$. Dashed line (top) shows theoretical value for ideal semispherical caps. Symbols/lines show values obtained with cutoff parameters $r_{c,\text{cap}} = 8l_b$ and $r_{c,\text{junction}} = 20l_b$. Grey shaded areas indicate spread of results if one varies the cutoff between $r_{c,\text{cap}} \in [7, 10]l_b$ and $r_{c,\text{junction}} \in [10, 25]l_b$.

separate the structures into “caps”, “junctions”, and “tubular” sections as indicated in Fig. 2b), extract an elastic energy e per tube length from the tubular sections, and evaluate the excess energies of caps and junctions via $\Delta E_{\text{cap,junction}} = E_{\text{cap,junction}} - l_{\text{ref}} e$, where $l_{\text{ref}} = A_{\text{cap,junction}}/2\pi R_T$ is the length of the reference tube section. For example, the ideal values for semispherical caps are $e = \pi\kappa/R_T$ and $\Delta E_{\text{cap}} = 3\pi\kappa$, and this is independent of the cutoff value r_c marking the end of the “cap” region as long as $r_c > R_T$. The procedure thus largely removes the dependence of the results on the specific dissection into junctions, caps, and tubular regions.

In practice, the results are still somewhat sensitive to the choice of the cutoff values r_c (Fig. 2d, shaded areas). Even taking these uncertainties into account, it is clear that the excess energy of caps is positive ($\Delta E_{\text{cap}} = 190$ – 220ϵ depending on the applied force) and the excess energy of junctions is negative ($\Delta E_{\text{junction}} \approx -280\epsilon$). The excess energy of caps is higher than the theoretical estimate $E_{\text{cap}} = 3\pi\kappa$, which we attribute to some extra distortion in the vicinity of the vertex where the force F_{ext} is applied. The negative excess energy of junctions reflects the fact that the overall curvature in the region of the junction is reduced. Interestingly, in branched structures, the energy gain at junctions more than compensates the energy loss due to the formation of an additional cap. As a result, the total elastic energy of branched structures is lower than that of linear structures.

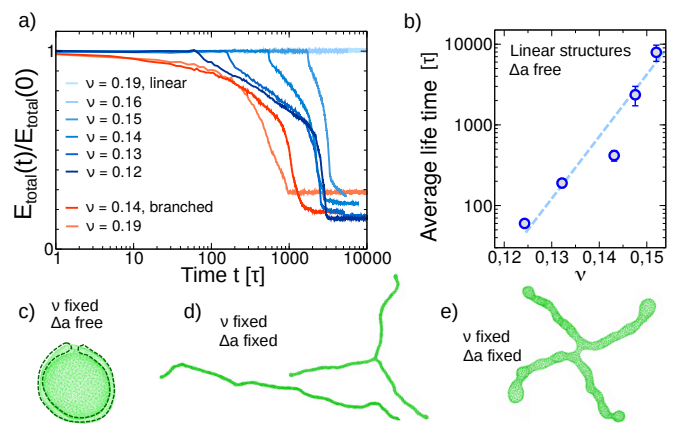


FIG. 3. Stability of force-free tubular structures. (a) Examples of time evolution of the total energy after releasing the force on force-stabilized linear (blue) and branched (red) structures at fixed ν as indicated (Δa is not constrained). Both structures eventually transform into a stomatocyte. For linear structures, the transformation process sets in after an activation time, which exceeds the maximum simulation time for $\nu > 0.15$. (b) Average life time of linear structures after releasing the stabilizing force as a function of ν (Δa is free). Dashed line shows exponential behavior. (c) Example of a stable stomatocyte structure with $\nu = 0.14$. (d) Stable linear and branched structure if both ν and Δa are fixed ($\nu = 0.14$). (e) Structure obtained after releasing the force from a force-stabilized tetrahedral structure at fixed ν and Δa (at $\nu = 0.2$). The tetra-junction splits up into two Y-junctions.

Force-free (meta)stable structures. We turn to the question whether branched structures can be metastable in the absence of forcing. Bahrami et al [43] have recently observed that linear structures remain metastable if the enclosed volume V_0 is fixed. Motivated by their findings, we study in Fig. 3a) the time evolution of linear and branched structures after releasing a stabilizing force while keeping V_0 fixed. In both cases, the structures eventually transform into a structure with lower energy, a stomatocyte (see Fig. 3c). However, the transformation process is qualitatively different. In branched structures, it sets in immediately via a disc-like widening at the junction (see SI movie `branch_fixNu.mp4`). Linear structures initially remain (meta)stable for some activation time, indicating that the shape change is an activated process. The transformation is then initiated by the nucleation of a disc at one end (see SI movie `linear_fixNu.mp4`). The activation time of linear structures increases roughly exponentially with ν (see Fig. 3b) and eventually exceeds the total simulation time, consistent with [43].

Imposing a small reduced volume alone is thus not sufficient to stabilize branched structures. However, constraining the average curvature Δa in addition to ν does have a stabilizing effect. SI Fig. 2a,b shows that Δa drops substantially during the transformation from tubular/branched structures to stomatocyte. If one constrains Δa to its initial value, i.e., the value of the force-stabilized structure, this suppresses the transformation,

and the tubular/branched structures with Y-junctions remain (meta)stable. Examples are shown in Fig. 3d). Tetrahedral junctions, on the other hand, do not persist, but separate into two Y-junctions (see Fig. 3d, SI Fig. 2e and SI movie `f0.tetrahedral_nu20fixDa.mp4`). If only Δa is kept fixed, linear and branched structures are also stable, but may acquire slightly pearled shapes, see SI Fig. 2d).

Origin of energy penalty for junction defects. The question remains which of the two structures, branched or linear, has the lower energy. Judging from our previous results on excess cap and junction energies (Fig. 2), one might suspect that branching is energetically favorable. However, the situation is more subtle. Adding a junction locally removes curvature in the junction region, which has to be added elsewhere to keep Δa fixed. As a result, the tubular sections become thinner, and their curvature energy increases. In SI, we present a theoretical estimate showing that the resulting net energy difference is roughly given by $E_{CV,branch} - E_{CV,linear} \sim \pi\kappa + |\varepsilon \cdot \Delta E_{CV,junction}| > 0$, where ε characterizes the reduction of curvature at the junction. At fixed Δa , the total curvature energy of branched structures should hence be higher than that of linear structures. A similar effect is expected for fixed ν : A junction adds enclosed volume, which has to be removed elsewhere, leading again to a thinning of tubes.

The net effect of constraints on the curvature energy as obtained from simulations is summarized in table I for the example of force-stabilized structures at $F_{ext} = 70\epsilon/l_b$. Here, we have used the values of ν and/or Δa obtained for unconstrained force-stabilized linear structures (parameter set C1) and branched structures (parameter set C2) as input parameters in constrained force-stabilized simulations of linear and branched structures. The curvature energies obtained with the set C1 are generally higher than those obtained with C2, because Δa is higher and/or ν is lower. Comparing linear and branched structures for the same parameter set, the results confirm the expectations of the discussion above. Only in the absence of any constraints is the curvature energy of branched structures lower than that of linear structures. In all other cases (constraints on ν , on Δa , on both), the curvature energy of branched structures is higher.

Conclusions. To summarize, we have investigated the energetics and stability of an essential component of tubular membrane networks, the junctions, from the point of view of the Canham-Helfrich elastic theory of membranes. We consider membrane structures with closed sphere topology and allow for constraints on the enclosed volume ν and the average curvature Δa , without however imposing specific local curvatures. Within this simple model, we find that Y-junctions with angles 120° can be stabilized by mechanical forces and remain metastable after releasing the forces. Other types of junctions and other angles are unstable. Furthermore, we find that Y-junctions locally have a negative excess curvature energy. For fixed tube diameter, branching is energeti-

Fixed	Structure	E_{CV}/ϵ		ν	Δa		
-	Linear	9333 ± 26		0.186 ± 0.001	3.90 ± 0.01		
	Branched	9082 ± 34		0.193 ± 0.001	3.81 ± 0.01		
		C1 (Linear)			C2 (Branched)		
		E_{CV}	ν	Δa	E_{CV}	ν	Δa
Δa	Linear	9333 ± 3	0.186	3.90	8975 ± 3	0.191	3.81
	Branched	9470 ± 3	0.187	3.90	9117 ± 3	0.192	3.81
ν	Linear	9355 ± 3	0.186	3.91	8882 ± 3	0.192	3.79
	Branch	9538 ± 4	0.186	3.92	9079 ± 4	0.193	3.80
$\nu, \Delta a$	Linear	9342 ± 3	0.186	3.90	8951 ± 3	0.192	3.81
	Branch	9480 ± 3	0.186	3.90	9126 ± 3	0.193	3.81

TABLE I. Curvature energies E_{CV} , reduced volumes ν , and average curvatures Δa for force-stabilized pure linear and branched structures at $F_{ext} = 70\epsilon/l_b$. Results are shown for two sets of constraints C1 and C2 on ν , Δa , or both as indicated, which correspond to the values obtained for unconstrained force-stabilized linear and branched structures, respectively.

cally favorable, even if one accounts for the positive energy of the additional cap. At fixed Δa , however, adding a branch enforces a thinning of the tubes, such that the overall curvature energy balance disfavors branching.

This subtle energy balance should lead to an increase of the lifetime of metastable branches, as their elimination is only favorable if the entire tube network rearranges. In addition, dynamical simulations suggest that the creation and annihilation of branches is accompanied by a free energy barrier: Pulling a branch out of a tube requires slightly higher forces than needed to stabilize it (see SI, Fig. 2a) and if one annihilates a branch by pulling on the other tubes, the curvature energy passes through a maximum (SI, Fig. 2b)

Our results thus indicate that simple properties of elastic membranes might be responsible for the abundance of tube network structures in cells. These structures are already metastable and long-lived if one imposes a few generic constraints, such as a fixed surface area difference between inner and outer membrane leaflet and possibly impermeability (fixed enclosed volume; not strictly necessary). Hence they can be stabilized and manipulated with little extra effort.

We have studied a very idealized model of bare membranes. However, given the generic character of our main conclusions, we expect them to still hold in other membrane models, e.g., ADE models with more realistic (lower) area difference elasticities $k_{\Delta a}$, or membrane structures with average curvature imposed by freely moving curvature-inducing proteins [19–24], where one has to account for their entropy of mixing. This will be an interesting subject for future studies.

We thank Enrico Schleiff for motivating this project, Hiroshi Noguchi from the ISSP at the University of Tokyo, Japan, for helpful discussions and for sharing the source code of his dynamically-triangulated membrane model [66], which was extended by us to include area difference constraints. The simulations were carried out on the supercomputer Mogon at Johannes Gutenberg

University Mainz. This work was funded by the state of Rhineland-Palatinate, Germany, within the Dynamem

consortium, and in part by the Deutsche Forschungsgemeinschaft (DFG) via Grant 233630050 (SFB TRR 146).

-
- [1] H. Mollenhauer and D. Morre, *Histochemistry and Cell Biology* **109**, 533 (1998).
- [2] M. De Matteis and A. Luini, *Nature reviews. Molecular cell biology* **9**, 273 (2008).
- [3] L. Westrate, J. Lee, W. Prinz, and G. Voeltz, *Annual Review of Biochemistry* **84**, 791 (2015), pMID: 25580528, <https://doi.org/10.1146/annurev-biochem-072711-163501>.
- [4] L. Lü, L. Niu, and J. Hu, *Biophysics Reports* **6** (2020), 10.1007/s41048-020-00113-y.
- [5] R. E. Powers, S. Wang, T. Y. Liu, and T. A. Rapoport, *Nature* **543**, 257 (2017).
- [6] J. Saraste and K. Prydz, *Frontiers in Cell and Developmental Biology* **7**, 171 (2019).
- [7] S. Sowinski, C. Jolly, O. Berninghausen, M. Purbhoo, A. Chauveau, K. Köhler, S. Oddos, P. Eissmann, F. Brodsky, C. Hopkins, B. Önfelt, Q. Sattentau, and D. Davis, *Nature Cell Biology* **10**, 211 (2008).
- [8] A. Roux, *Soft Matter* **9**, 6726 (2013).
- [9] H. Miyata and H. Hotani, *Proceedings of the National Academy of Sciences* **89**, 11547 (1992), <https://www.pnas.org/content/89/23/11547.full.pdf>.
- [10] H. Miyata, S. Nishiyama, K.-i. Akashi, and K. Kinoshita, *Proceedings of the National Academy of Sciences* **96**, 2048 (1999), <https://www.pnas.org/content/96/5/2048.full.pdf>.
- [11] I. Derényi, F. Jülicher, and J. Prost, *Phys. Rev. Lett.* **88**, 238101 (2002).
- [12] G. Koster, M. VanDuijn, B. Hofs, and M. Dogterom, *Proceedings of the National Academy of Sciences* **100**, 15583 (2003), <https://www.pnas.org/content/100/26/15583.full.pdf>.
- [13] C. Leduc, O. Campàs, K. B. Zeldovich, A. Roux, P. Jolimaitre, L. Bourel-Bonnet, B. Goud, J.-F. Joanny, P. Bassereau, and J. Prost, *Proceedings of the National Academy of Sciences* **101**, 17096 (2004), <https://www.pnas.org/content/101/49/17096.full.pdf>.
- [14] O. Campàs, C. Leduc, P. Bassereau, J. Casademunt, J.-F. Joanny, and J. Prost, *Biophysical Journal* **94**, 5009 (2008).
- [15] R. Nambiar, M. R. E., and M. J. Tyska, *PNAS* **106**, 11972 (2009).
- [16] W. Du, Q. Su, Y. Chen, Y. Zhu, D. Jiang, Y. Rong, S. Zhang, Y. Zhang, H. Ren, C. Zhang, X. Wang, N. Gao, Y. Wang, L. Sun, Y. Sun, and L. Yu, *Developmental Cell* **37**, 326 (2016).
- [17] M. J. Footer, J. W. J. Kerssemakers, J. A. Theriot, and M. Dogterom, *Proceedings of the National Academy of Sciences* **104**, 2181 (2007), <https://www.pnas.org/content/104/7/2181.full.pdf>.
- [18] A. Roux, G. Koster, M. Lenz, B. Sorre, J.-B. Manneville, P. Nassoy, and P. Bassereau, *Proceedings of the National Academy of Sciences* **107**, 4141 (2010), <https://www.pnas.org/content/107/9/4141.full.pdf>.
- [19] I. Tsafrir, Y. Caspi, M.-A. Guedeau-Boudeville, T. Arzi, and J. Stavans, *Phys. Rev. Lett.* **91**, 138102 (2003).
- [20] Y. Shibata, J. Hu, M. M. Kozlov, and T. A. Rapoport, *Annual Review of Cell and Developmental Biology* **25**, 329 (2009).
- [21] F. Campelo, H. T. McMahon, and M. M. Kozlov, *Biophysical Journal* **95**, 2325 (2008).
- [22] A. Frost, V. M. Unger, and P. De Camilli, *Cell* **137**, 191 (2009).
- [23] G. K. Voeltz, W. A. Prinz, Y. Shibata, J. M. Rist, and T. A. Rapoport, *Cell* **124**, 573 (2006).
- [24] J. Hu, Y. Shibata, C. Voss, T. Shemesh, Z. Li, M. Coughlin, M. M. Kozlov, T. A. Rapoport, and W. A. Prinz, *Science* **319**, 1247 (2008), <https://science.sciencemag.org/content/319/5867/1247.full.pdf>.
- [25] T. Shemesh, R. W. Klemm, F. B. Romano, S. Wang, J. Vaughan, X. Zhuang, H. Tukachinsky, M. M. Kozlov, and T. A. Rapoport, *Proceedings of the National Academy of Sciences* **111**, E5243 (2014), <https://www.pnas.org/content/111/49/E5243.full.pdf>.
- [26] U. Seifert and R. Lipowsky, *Structure and Dynamics of Membranes* **1**, 403 (1995).
- [27] N. Ramakrishnan, R. P. Bradleh, R. W. Tourdot, and R. Radhakrishnan, *J. Phys.: Cond. Matter* **30**, 273001 (2018).
- [28] R. Lipowsky, *Advanced Biology* **6**, 2101020 (2021).
- [29] P. Canham, *Journal of Theoretical Biology* **26**, 61 (1970).
- [30] W. Helfrich, *Zeitschrift für Naturforschung* **28C**, 693 (1973).
- [31] E. A. Evans, *Biophysical journal* **14**, 923–931 (1974).
- [32] U. Seifert, K. Berndl, and R. Lipowsky, *Phys. Rev. A* **44**, 1182 (1991).
- [33] G. Gompper and D. M. Kroll, *Phys. Rev. E* **51**, 514 (1995).
- [34] C. Vanhille-Campos and A. Saric, *Soft matter* **17**, 3798 (2021).
- [35] L. Bo and R. Waugh, *Biophysical journal* **55** **3**, 509 (1989).
- [36] D. J. Bukman, J. H. Yao, and M. Wortis, *Phys. Rev. E* **54**, 5463 (1996).
- [37] C. R. Calladine and J. A. Greenwood, *J. of Biomech. Eng. – Trans. of the ASME* **124**, 576 (2002).
- [38] A.-S. c. v. Smith, E. Sackmann, and U. Seifert, *Phys. Rev. Lett.* **92**, 208101 (2004).
- [39] G. Koster, A. Cacciuto, I. Derényi, D. Frenkel, and M. Dogterom, *Phys. Rev. Lett.* **94**, 068101 (2005).
- [40] I. Golushko and S. Rochal, *Journal of Experimental and Theoretical Physics* **122**, 169 (2016).
- [41] H. Noguchi, *Soft Matter* **17**, 10469 (2021).
- [42] A. Paraschif, T. J. Lagny, C. Vanhille-Campos, E. Coudrier, P. Bassereau, and A. Saric, *Biophysical Journal* **120**, 598 (2021).
- [43] A. H. Bahrami and G. Hummer, *ACS Nano* **11**, 9558 (2017).
- [44] W. Rawicz, K. Olbrich, T. McIntosh, D. Needham, and E. Evans, *Biophysical Journal* **79**, 328 (2000).
- [45] M. D. Carmo, *Differential Geometry of Curves and Surfaces* (Prentice Hall, 1976).
- [46] B. Bozic, S. Svetina, B. Zeks, and R. Waugh, *Biophysical*

journal **61**, 963–973 (1992).

- [47] W. Wiese, W. Harbich, and W. Helfrich, *Journal of Physics: Condensed Matter* **4**, 1647 (1992).
- [48] V. Heinrich, S. c. v. Svetina, and B. c. v. Žekš, *Phys. Rev. E* **48**, 3112 (1993).
- [49] L. Miao, U. Seifert, M. Wortis, and H.-G. Döbereiner, *Phys. Rev. E* **49**, 5389 (1994).
- [50] M. Sheetz and S. Singer, *Proceedings of the National Academy of Sciences of the United States of America* **71**, 4457–4461 (1974).
- [51] S. Svetina and B. Zeks, *European biophysics journal : EBJ* **17**, 101–111 (1989).
- [52] P. Zihlerl and S. Svetina, *Europhysics Letters (EPL)* **70**, 690 (2005).
- [53] Itzykson, *Proceedings of the GIFT seminar, Jaca85, WorldScientific, Singapore* (1986).
- [54] Y. Kantor and D. R. Nelson, *Phys. Rev. Lett.* **58**, 2774 (1987).
- [55] G. Gompper and D.M. Kroll, *J. Phys. I France* **6**, 1305 (1996).
- [56] G. Gompper and D. M. Kroll, *Journal of Physics: Condensed Matter* **9**, 8795 (1997).
- [57] F. Jülicher, *Journal de Physique II* **6**, 1797 (1996).
- [58] A. Šarić and A. Cacciuto, *Phys. Rev. Lett.* **109**, 188101 (2012).
- [59] A. H. Bahrami, R. Lipowsky, and T. R. Weigl, *Phys. Rev. Lett.* **109**, 188102 (2012).
- [60] N. Ramakrishnan, P. Sunil Kumar, and J. H. Ipsen, *Biophysical Journal* **104**, 1018–1028 (2013).
- [61] A. Vahid, A. Šarić, and T. Idema, *Soft Matter* **13**, 4924 (2017).
- [62] B. Li and S. M. Abel, *Soft Matter* **14**, 185 (2018).
- [63] M. Hoore, F. Yaya, T. Podgorski, C. Wagner, G. Gompper, and D. A. Fedosov, *Soft Matter* **14**, 6278 (2018).
- [64] X. Bian, S. Litvinov, and P. Koumoutsakos, *Computer Methods in Applied Mechanics and Engineering* **359**, 112758 (2020).
- [65] H. Noguchi and G. Gompper, *Phys. Rev. Lett.* **93**, 258102 (2004).
- [66] H. Noguchi and G. Gompper, *Phys. Rev. E* **72**, 011901 (2005).
- [67] T. Lobovkina, P. Dommersnes, J. F. Joanny, P. Bassereau, M. Karlsson, and O. Orwar, *Proceedings of the National Academy of Sciences of the United States of America* **101** **21**, 7949 (2004).
- [68] T. Lobovkina, P. Dommersnes, J.-F. Joanny, J. Hurtig, and O. Orwar, *Phys. Rev. Lett.* **97**, 188105 (2006).
- [69] T. Lobovkina, P. Dommersnes, S. Tiourine, J. Joanny, and O. Orwar, *The European physical journal. E, Soft matter* **26**, 295 (2008).
- [70] A small compensating force is applied to all N vertices to ensure that the total force is still zero.
- [71] F. H. Stillinger and T. A. Weber, *Phys. Rev. B* **31**, 5262 (1985).
- [72] The area difference ΔA is usually given by $\Delta A = 2h \int dA K$, where h is the thickness of the membrane[64]. However, different conventions exist[31, 43, 46–51, 64], which makes it more convenient to use the renormalized area difference Δa that is one for a sphere.

Supplementary Information

A. Dynamically-triangulated membrane model

For the simulations the dynamically-triangulated membrane model of Ref. [66] was used. The model is described in detail in that reference. Here we briefly recapitulate the potentials and parameters for the convenience of the reader.

Curvature Energy

The shape of the vesicle is mostly controlled by the curvature energy given by Eq. (1) in the main text. This equation is discretized as follows [53, 55]:

$$U_{cv} = \frac{\kappa}{2} \sum_i \frac{1}{\sigma_i} \left(\sum_{j(i)} \frac{\sigma_{i,j} \vec{r}_{i,j}}{r_{i,j}} \right)^2 \quad (2)$$

The value for the bending rigidity for lipid membranes is typically $\kappa = 20 k_B T$ [44], where $k_B T$ is the thermal energy. The first sum goes over all vertices i and the second sum goes over all neighbors of the vertex i , $j(i)$, that are connected by bonds. The vector between vertices i and j is denoted by $\vec{r}_{i,j}$ and $r_{i,j} = \|\vec{r}_{i,j}\|$. $\sigma_{i,j}$ is the length of the bond in the dual lattice, which is given by $\sigma_{i,j} = r_{i,j}[\cot(\theta_1) + \cot(\theta_2)]/2$, where θ_1 and θ_2 are the angles opposite to the bond connecting i and j in the two triangles sharing this bond. The area of the dual cell of vertex i is given by $\sigma_i = 0.25 \sum_{j(i)} \sigma_{i,j} r_{i,j}$.

Bond and Repulsive Interactions

In order to perform molecular dynamics simulations a Stillinger-Weber potential [71] is used to describe bond and excluded-volume interactions between vertices. All vertices connected by bonds interact via the following attractive potential:

$$U_{\text{bond}}(r_{i,j}) = \varepsilon \begin{cases} \frac{l_b \exp[l_b/(l_{c0} - r_{i,j})]}{l_{\text{max}} - r_{i,j}} & (r_{i,j} > l_{c0}) \\ 0 & (r_{i,j} \leq l_{c0}). \end{cases} \quad (3)$$

At short distances all particles interact via the following repulsive excluded volume potential:

$$U_{\text{rep}}(r_{i,j}) = \varepsilon \begin{cases} \frac{l_b \exp[l_b/(r_{i,j} - l_{c1})]}{r_{i,j} - l_{\text{min}}} & (r_{i,j} < l_{c1}) \\ 0 & (r_{i,j} \geq l_{c1}) \end{cases} \quad (4)$$

The parameters of the potentials are listed in Table II, where the parameter l_b refers to the bond length and the parameter $\varepsilon = 80 k_B T$ is a constant energy prefactor.

This bond length is the length unit and hence set to one in all simulations.

Parameter	Value	Description
l_{\max}	$1.33l_b$	maximum bond length
l_{\min}	$0.67l_b$	minimum distance between two vertices
l_{c0}	$1.15l_b$	cutoff length for U_{bond}
l_{c1}	$0.85l_b$	cutoff length for U_{rep}

TABLE II. Parameters used for the bond and repulsive interactions.

Area and Volume

The total area is the sum over the area of each vertex A_i , which is given by the weighted sum over the area of all neighboring triangles A_α :

$$A = \sum_{i=1}^N A_i \quad \text{with} \quad A_i = \frac{1}{3} \sum_{\alpha \in \text{neigh. triangles}} A_\alpha \quad (5)$$

Here and in the following quantities with greek indices denote triangles and roman indices denote vertices.

The volume V enclosed by the membrane is calculated as [43]:

$$V = \sum_{\alpha=1}^{N_t} V_\alpha \quad \text{with signed subvolumes} \quad V_\alpha = \frac{1}{3} (\hat{n}_\alpha \cdot \vec{R}_\alpha) A_\alpha, \quad (6)$$

where \hat{n}_α is the unit normal vector of triangle α pointing outwards and \vec{R}_α is the position vector of one of the vertices of the triangle relative to an a reference point. This reference point can, in fact, be chosen arbitrarily and can even lie outside of the structure, because any additional contribution from outside the vesicle will eventually be subtracted by another subvolume V_α .

Area Difference

The renormalized area difference [72] Δa is defined as:

$$\Delta a = \frac{1}{4\sqrt{\pi A_0}} \int dAK = \frac{1}{4\sqrt{\pi A_0}} \sum_{i=1}^N |\vec{H}_i| \frac{\vec{H}_i \cdot \hat{n}_i}{|\vec{H}_i \cdot \hat{n}_i|} \quad (7)$$

where \vec{H}_i is the oriented curvature contribution of vertex i ,

$$\vec{H}_i = \sum_{j(i)} \frac{\sigma_{i,j} \vec{r}_{i,j}}{r_{i,j}}. \quad (8)$$

Here, the term $\vec{H}_i \cdot \hat{n}_i / |\vec{H}_i \cdot \hat{n}_i|$ gives the orientation of the curvature, i.e. if it is convex (+1) or concave (-1) using the surface normal vector \hat{n}_i , as the average orientation of the neighboring triangles. The normalization is chosen such that a sphere has an area difference of $\Delta a = 1$.

Constraint Potentials

In our simulations, the area A of branched and linear structures is constrained to $A = A_0$ by introducing a constraint potential

$$U_A = \frac{1}{2} k_A (A - A_0)^2. \quad (9)$$

In some simulations, additional constraint potentials U_V and/or $U_{\Delta a}$ are included to fix the enclosed volume at $V = V_0$ via

$$U_V = \frac{1}{2} k_V (V - V_0)^2 \quad (10)$$

and/or the renormalized area difference Δa at Δa_0 via

$$U_{\Delta a} = \frac{1}{2} k_{\Delta a} (\Delta a - \Delta a_0)^2. \quad (11)$$

Since the constraints are implemented by harmonic potentials rather than being strictly enforced, small variations in A , V , and Δa are still possible even in the presence of constraint potentials. For example, in Table 1 of the main text, the actual values sometimes slightly differ (by less than 1%) from the imposed values.

Overall Potential

Finally, the overall potential used in the simulations is a combination of all the potentials described above:

$$U_{\text{tot}} = U_{\text{cv}} + U_{\text{bond}} + U_{\text{rep}} + U_A + U_V + U_{\Delta a} \quad (12)$$

The total Hamiltonian of the system is therefore:

$$H_0 = \sum_{i=1}^N \frac{\vec{p}_i^2}{2m} + U_{\text{tot}} \quad (13)$$

where \vec{p}_i are the momenta of the vertices and m their masses.

B. Time evolution, transformation pathways, and movies

1. Higher order junctions subject to external forces

As mentioned in the main text, higher order junctions tend to split up into Y-junctions in the simulations with applied mechanical force. Fig. 4a,b) shows an example of such an evolution. The following movies are provided along with this article to illustrate this further:

- **4fold.mp4**: Time evolution after applying four coplanar forces with angles 90° (Fig. 4b).
- **4fold_twisted.mp4**: Time evolution after applying four forces with angles 90° , which are twisted with respect to each other.

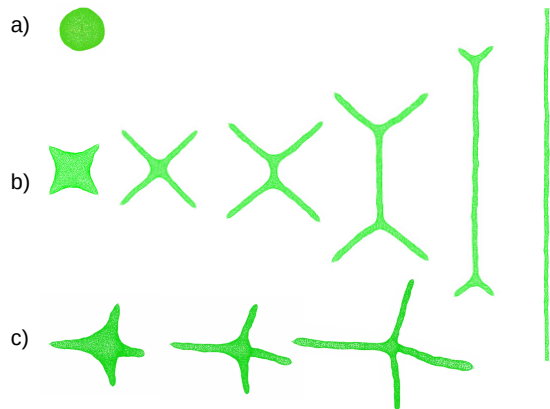


FIG. 4. Time evolution of mechanically enforced tubular structures with intermediate higher order junctions. (a) Initial state: A small sphere (no volume constraint). (b) Evolution after applying four forces F_{ext} in a plane with angle 90° . First a four-fold junction forms. Then this junction separates into two Y-junctions. Since they do not have the correct angles 120° , they move outwards. The final stable state is a tube. The same behavior is observed if the forces on the branches are twisted with respect to each other (not shown). (c) Evolution if the four forces F_{ext} are applied in tetrahedral direction. In this case, a tetrahedral quadruple-junction forms and remains stable.

- **tetrahedral.mp4**: Time evolution after applying four forces with with angles corresponding to a tetrahedral junction. Under the influence of external forces, the tetrahedral junction is stable (Fig. 4c).

2. Force-free structures

As explained in the main article, branched structures and thin linear structures undergo a transformation to a stomatocyte structure if the stabilizing forces are released at fixed reduced volume ν . This is shown in the following movies:

- **f0_branch_nu14.mp4**: Time evolution after releasing the forces from an initially branched structure with a Y-junction while keeping $\nu = 0.14$ fixed. The transition sets in instantaneously.
- **f0_branch_nu19.mp4**: Time evolution after releasing the forces from an initially branched structure with a Y-junction while keeping $\nu = 0.19$ fixed. The transition sets in instantaneously.
- **f0_linear_nu14.mp4**: Time evolution after releasing the forces from an initially linear structure while keeping $\nu = 0.14$ fixed. The transition sets in after an activation time.

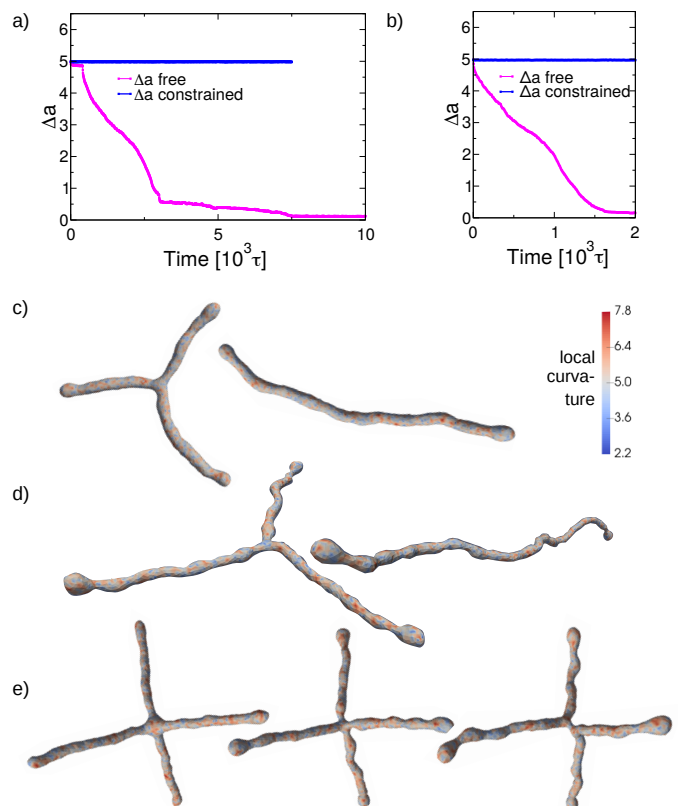


FIG. 5. (a,b) Time evolution of the rescaled area difference Δa after releasing the force on a force-stabilized linear (a) and branched (b) structure at fixed reduced volume $\nu = 0.14$ (pink curve). If Δa is kept fixed (blue curve), the tubular-stomatocyte transformation is suppressed, and the linear and branched structures persist. (c) Examples of force-free metastable linear and branched structures for fixed $\nu = 0.27$ and fixed Δa . (d) Examples of stable structures for fixed Δa and unconstrained ν (e) Time evolution of an initially force-stabilized structure containing a tetrahedral junction at fixed $\nu = 0.2$ and Δa . The tetrahedral junction splits up into two Y-junctions. The color coding in c-e) indicates distribution of local curvature on the surfaces.

- **f0_linear_nu19.mp4**: Time evolution after releasing the forces from an initially linear structure while keeping $\nu = 0.19$ fixed. Within the simulation time, no transition takes place.

Constraining the average curvature Δa in addition to the reduced volume ν stabilizes the tubular structures, and both linear and branched tubular structures remain stable (see Fig. 5 a-d). Tetrahedral junctions however do not survive, they split up into two Y-junctions. This is shown in Fig. 5e) and in the movie **f0_tetrahedral_nu20fixDa.mp4**.

C. Curvature energy balance of tubular structures at fixed Δa

We wish to estimate the energy difference between pure tubes and branched structures with three arms under the condition that the area difference, $\Delta a \propto I_K := \int dA K$ is fixed.

First we estimate the local excess energies of caps and junctions.

Our reference system is a pure cylinder (no caps) with area A and tube radius R , which has the curvature energy $E_{CV} = A/2R^2$ and the integrated curvature $I_K = A/R$. Compared to this reference, each spherical cap contributes an excess free energy $\Delta E_{\text{cap}} = 3\pi\kappa$ and an excess integrated curvature $\Delta I_{K,\text{cap}} = 2\pi R$. Correspondingly, each junction contributes an excess free energy $\Delta E_{\text{junction}}$ and an excess integrated curvature $\Delta I_{K,\text{junction}}$, which are both unknown. However, we can approximately relate them to each other by assuming that the junction can be described as a section with area A_{junction} with reduced mean total curvature α/R , $\alpha < 1$. This implies

$$\Delta I_{K,\text{junction}} \approx (\alpha - 1) \frac{A_{\text{junction}}}{R}, \quad (14)$$

$$\Delta E_{\text{junction}} \approx (\alpha^2 - 1)\kappa \frac{A_{\text{junction}}}{2R^2} \quad (15)$$

From Fig. 2c in the main article, we know $\Delta E_{\text{junction}} \approx -280$, roughly independent of the tube radius, hence $\alpha < 1$ and $A_{\text{junction}}/R^2 =: a_{\text{junction}} \approx \text{const.}$

The curvature energy and the integrated curvature of tubes and three-arm structures with radius R are estimated as

$$\frac{1}{\kappa} E_{CV,\text{tube}} = \frac{A}{2R^2} + 6\pi \quad (16)$$

$$\frac{1}{\kappa} E_{CV,\text{branch}} = \frac{A}{2R^2} + 9\pi + \frac{\Delta E_{\text{junction}}}{\kappa} \quad (17)$$

$$I_{K,\text{tube}} = \frac{A}{R} + 4\pi R \quad (18)$$

$$I_{K,\text{branch}} = \frac{A}{R} + 6\pi R + \Delta I_{K,\text{junction}} \quad (19)$$

For given fixed R , the curvature energy of branched structures and pure tubes thus differs by

$$E_{CV,\text{branch}} - E_{CV,\text{tube}} = 3\pi\kappa + \Delta E_{\text{junction}} \approx -90 \quad (20)$$

which is negative as discussed in the main article.

However, if I_K is kept fixed, then both the radii of the pure tube, R_{tube} and of the branched structure, R_{branch} , change with respect to the value \bar{R} in the reference cylinder. Denoting $\bar{c} = 1/\bar{R}$ and $\Delta c = 1/R - 1/\bar{R}$, Eq. (18) yields

$$\Delta c_{\text{linear}} = -\frac{4\pi}{A} R_{\text{linear}} \quad (21)$$

for linear structures, and Eq. (19)

$$\Delta c_{\text{branch}} = -\frac{1}{A} \left(6\pi R_{\text{branch}} + \Delta I_{K,\text{branch}} \right) \quad (22)$$

for branched three-arm structures. Inserting this in Eqs. (16), (17), we obtain

$$\begin{aligned} \frac{1}{\kappa} E_{CV,\text{linear}} &= \frac{A}{2} (\bar{c} + \Delta c)^2 + 6\pi \\ &= \frac{A}{2} \bar{c}^2 + 2\pi + \mathcal{O}\left(\frac{1}{A}\right) \end{aligned} \quad (23)$$

$$\begin{aligned} \frac{1}{\kappa} E_{CV,\text{branch}} &= \frac{A}{2} (\bar{c} + \Delta c)^2 + 9\pi + \frac{\Delta E_{\text{junction}}}{\kappa} \\ &= \frac{A}{2} \bar{c}^2 + 3\pi + \frac{a_{\text{junction}}}{2} (\alpha - 1)^2 \\ &\quad + \mathcal{O}\left(\frac{1}{A}\right) \end{aligned} \quad (24)$$

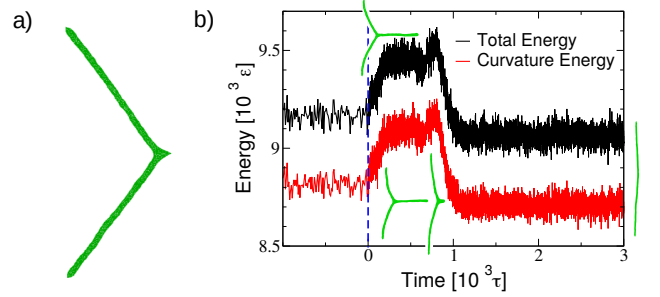


FIG. 6. Transition between linear and branched structures (a) Metastable configuration of a linear tubular structure when applying a force to pull a branch out from the tubular structure, using the same external forces as needed to stabilize branches. The tube deforms, but does no branch emerges. ($F_{\text{ext}} = 90$, no constraints). (b) Time evolution after releasing the force on one tube in a branched structure and pulling the other two tubes with in opposite directions ($F_{\text{ext}} = 70$). Δa and ν are constrained to fixed values. The force is released at the time $t = 0$. It retracts and eventually disappears at the time $t \approx 2 \times 10^3 \tau$. During this process, the curvature energy rises, suggesting the presence of a free energy barrier.

where we have used $R_{\text{linear/branch}} \bar{c} = 1 + \mathcal{O}(1/A)$ and Eqs. (14,15). Hence the difference between the energy of branched and linear structures for fixed area difference is approximated by

$$E_{CV,\text{branch}} - E_{CV,\text{linear}} \approx \pi\kappa + \frac{\kappa}{2} a_{\text{junction}} (\alpha - 1)^2 \quad (25)$$

which is now always positive. In terms of $\Delta E_{CV,\text{junction}}$, this expression can be rewritten as

$$E_{CV,\text{branch}} - E_{CV,\text{linear}} = \pi\kappa + |\varepsilon \cdot \Delta E_{CV,\text{junction}}|. \quad (26)$$

with $\varepsilon = (1 - \alpha)/(1 + \alpha)$.

We should note that the final result does not depend on the sign of $\Delta E_{\text{junction}}$. The underlying reason is that it is always more favorable to distribute a given integrated curvature as homogeneously as possible on a fixed surface than to allow for local variations.

D. Transitions between pure linear and branched structures

To investigate transitions between linear and branched structures, we have carried out two types of simulations.

First, starting from a force-stabilized linear tubular structure, we apply forces F_{ext} at the tube ends and an additional point in the middle with angles 120° . The tube deforms and assumes a V-shape, but no branch forms out (Fig. 6a). In order to pull an additional branch out, the additional force must be increased by $\Delta F_{\text{ext}} \approx 3 - 4$,

which is approximately 4-6% higher than the force needed for stabilization (at $F_{\text{ext}} = 60 - 1000$).

Second starting from a force-stabilized branched structure, we release the force on one branch and replace the forces on the other two ends by two forces F_{ext} in opposite direction. This is done at fixed Δa and ν . The loose branch retracts and eventually vanishes. This is associated with an increase of curvature energy (Fig. 6b). A similar barrier is observed if only ν is kept fixed. If both ν and Δa are unconstrained, no energy barrier is observed, instead the curvature energy even drops during the transition.